SUPPLEMENTARY INFORMATION

To show the partial encapsulation of nm-Si in the rGO matrix more clearly, we do show an enlarged image from **Figure 2 d** in the manuscript in higher resolution here (**Figure S1**).

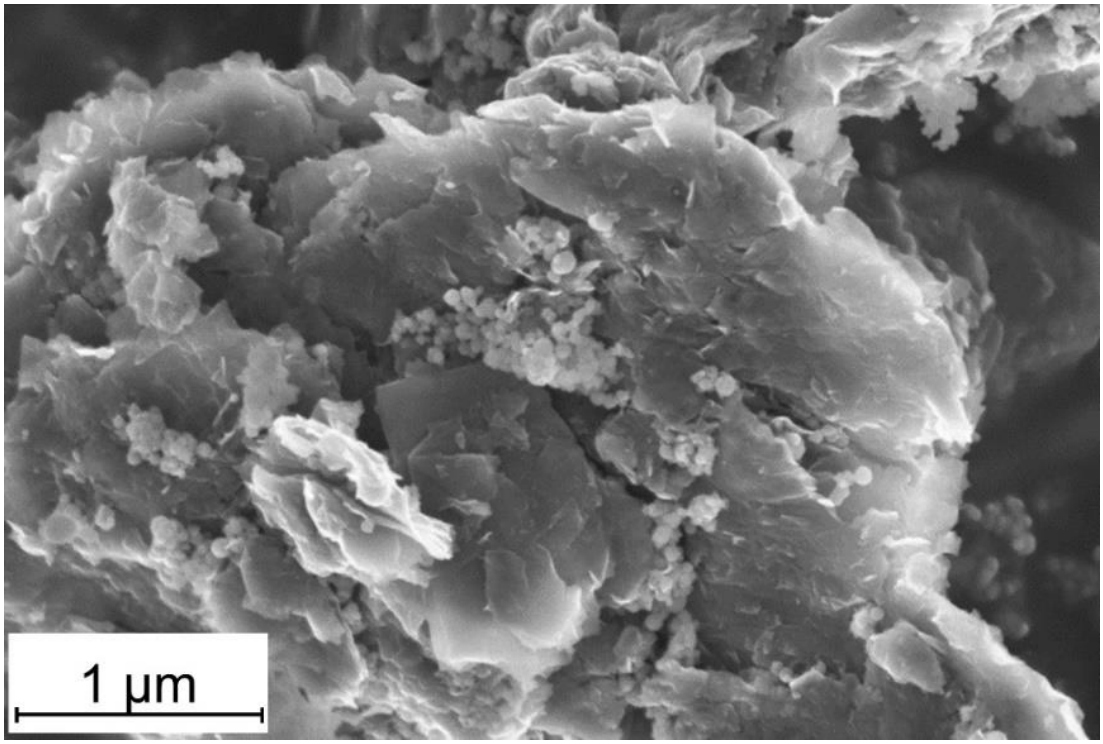

***Figure S1**: Enlarged SEM micrograph (SE) of nm-Si-rGO at a magnification of 25000x.*

Next to the EIS measurements of the pristine electrodes to detect the electrical conductivities (Figure 7), we performed galvanostatic EIS on the corresponding half cells (f = 1 MHz to 0.5 Hz, I = 0.2 mA). The results are summarized in **Table S1**.

***Table S1**: Inner resistances of the different electrodes before and after cycling (71 full cycles) obtained from GEIS measurements (f = 1 MHz – 0.5 Hz; I = 0.2 mA).*

Binder ratio	**Inner Resistance R_i in Ω**					
	nm-Si-rGO		µm-Si-rGO		rGO	
	before	after	before	after	before	after
3.75CMC_1.25SBR	3.06 ± 0.07	9.43 ± 0.59	3.32 ± 0.41	9.78 ± 1.61	-	-
2.5CMC_2.5SBR	3.24 ± 0.24	9.13 ± 0.64	3.46 ± 0.96	11.00 ± 4.39	2.85 ± 0.20	7.27 ± 0.20
1.25CMC_3.75SBR	3.42 ± 0.30	10.06 ± 1.17	3.00 ± 0.36	10.66 ± 2.02	-	-

These measurements confirm the conductivity measurements, as in general no significant differences can be seen. In all the Si-containing cells examined, the internal resistance increases by about three times after 71 cycles as a result of the different degradation mechanisms. The differences between µm- and nm-Si are small. The Si-free rGO electrode shows lower internal resistances both before and after cycling, with the difference being higher after cycling. It can be assumed that this is due to the thinner and less developed SEI. The detailed curves of the corresponding EIS measurements are additionally shown in **Figure S12**.

To better understand the results of the Si-rGO cells, we additionally show the Si-free rGO cycling in **Figure S2**.

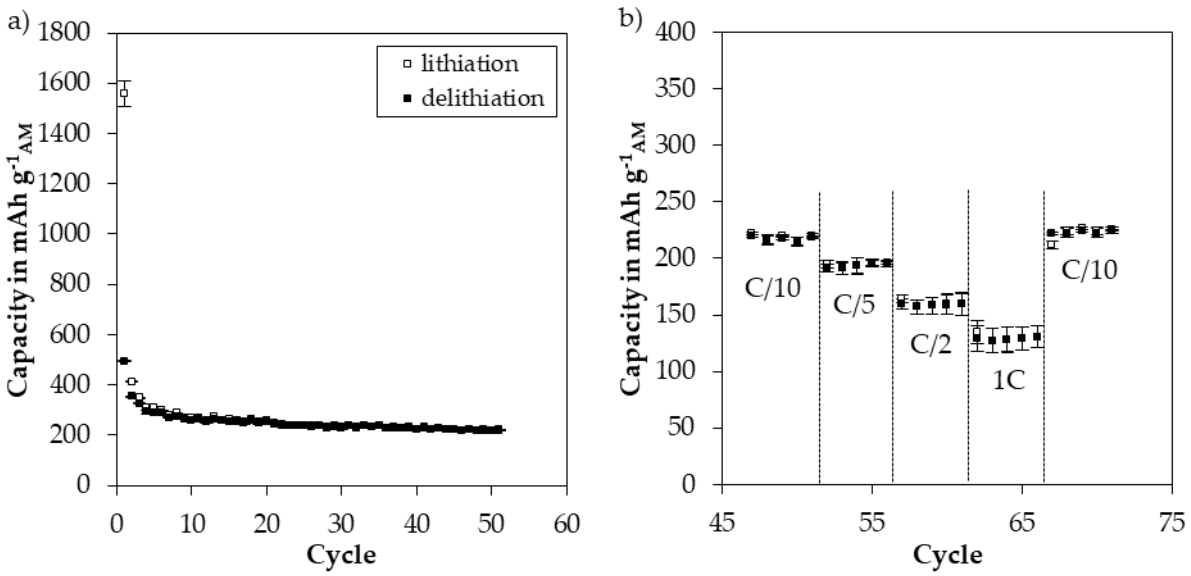

***Figure S2**: Specific delithiation and lithiation capacities of the Si-free rGO electrode: a) Constant current cycling at 0.1 C rate for 51 cycles and b) C-rate variation at 0.1 C, 0.2 C, 0.5 C and 1 C.*

A very high irreversible capacity can be seen for the first lithiation due to the high specific surface area and the remaining oxygen-containing groups as a result of the reaction with the electrolyte components during SEI formation. After approximately five (formation) cycles, a rather stable cycling behavior can be observed. The capacities at higher C-rates are significantly better than those of the Si-containing cells. This again confirms the less developed passivation layer (see **Table S1**). In addition, the charge and discharge curves of the Si-free rGO electrode are given in **Figure S11**.

In addition to the delithiation capacities shown in the manuscript (**Figure 8, 9 and 10**), we present the lithiation capacities for the Si-containing electrodes in **Figure S3 and S4**.

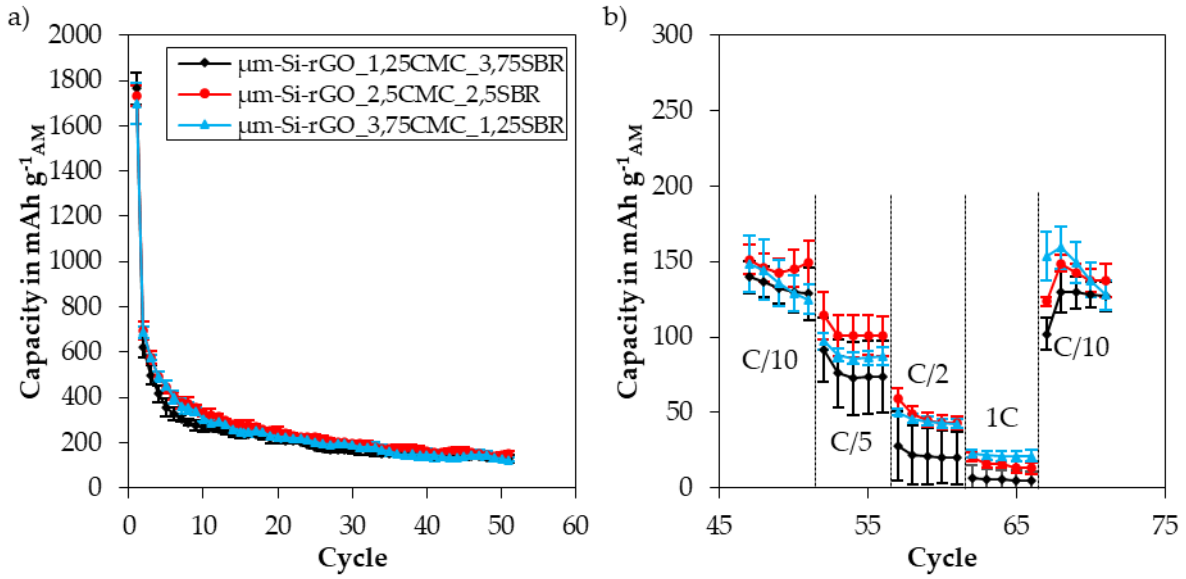

Figure S3: Specific lithiation capacities of the µm-Si-rGO electrodes: a) Constant current cycling at 0.1 C rate for 51 cycles and b) C-rate variation at 0.1 C, 0.2 C, 0.5 C and 1 C.

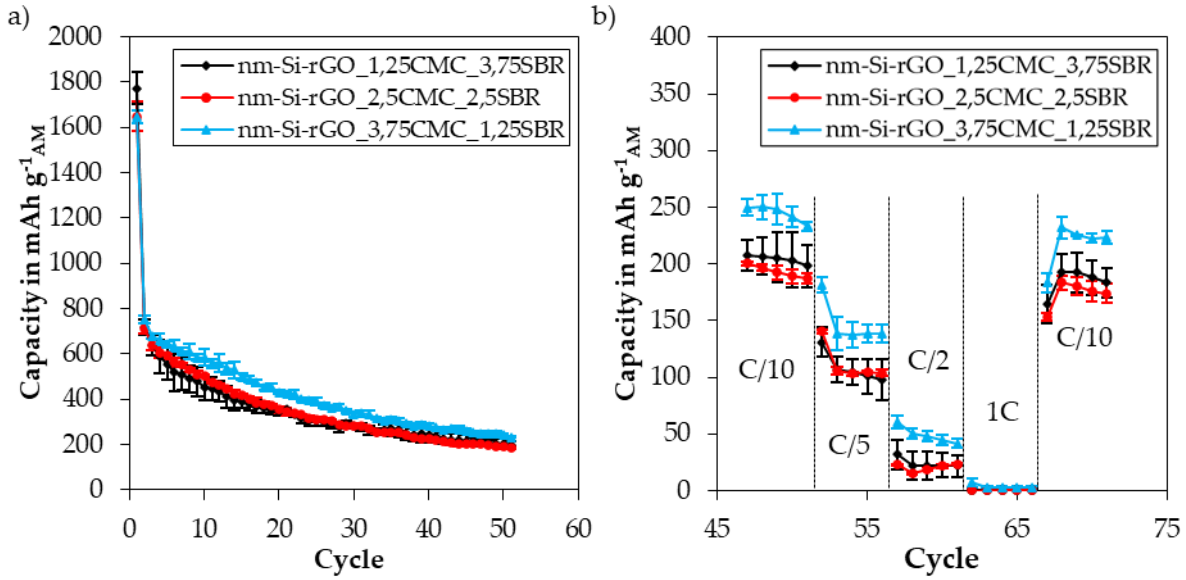

Figure S4: Specific lithiation capacities of the nm-Si-rGO electrodes: a) Constant current cycling at 0.1 C rate for 51 cycles and b) C-rate variation at 0.1 C, 0.2 C, 0.5 C and 1 C.

In general, the same trends can be observed for the lithiation as for the delithiation capacities and no indications of irreversible reactions, such as Li plating, can be seen. In general. high lithiation capacities can be found in cycle 1 for all electrodes investigated independent on the Si particle size or the binder composition. This is mainly due to the high surface area of the rGO matrix as it can also be seen for the Si-free electrode (see above). The high surface area leads to a high electron consumption during the first lithiation process as a result of irreversible SEI formation. Remaining oxygen containing groups in the rGO additionally enhance this effect.

Furthermore, we want to show the differences of the electrode structure before and after cycling dependent on the Si particle size in **Figure S5**.

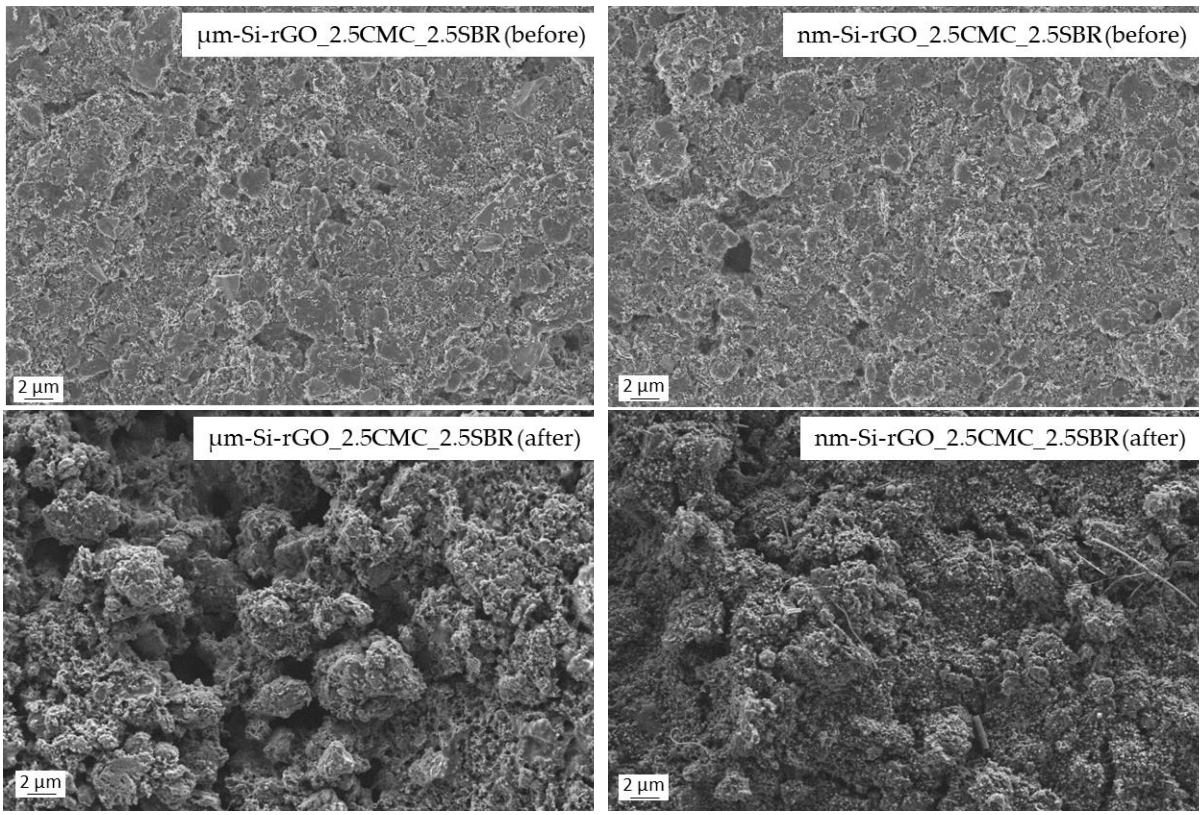

***Figure S5**: SEM micrographs of µm-Si-rGO_2.5CMC_2.5SBR and nm-Si-rGO_2.5CMC_2.5SBR before and after cycling.*

Before cycling for both electrodes a very similar and low-porous coating can be observed. From the post-mortem SEM images can be seen that the µm-Si-rGO electrode obtains a significant higher porosity compared to the nm-Si-rGO electrode after cycling due to the high volume increase during lithiation followed by the shrinkage during delithiation. Here, only the 2.5CMC_2,5SBR samples are shown, as the other binder compositions do not differ.

To present the degradation of the different Si-rGO electrodes more clearly, we modelled the differential capacities for the cycles 5, 10, 20, and 50 from the (de-) lithiation curves. In **Figure S6** the results of the µm-Si-rGO electrodes are given. The differential capacities are calculated from the charge and discharge curves (see **Figure S9**).

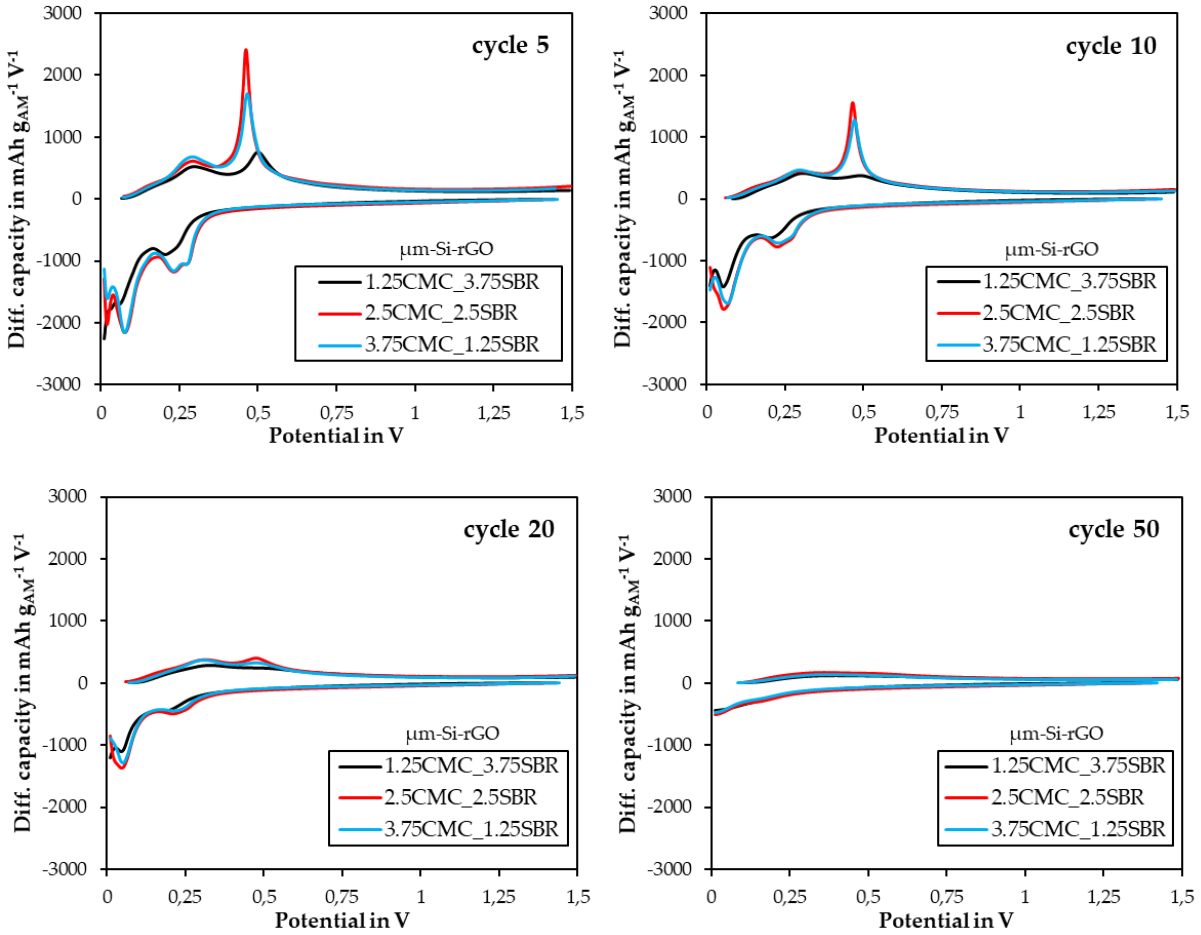

Figure S6: Differential capacity over potential for all µm-Si-rGO electrodes for cycle 5, 10, 20 and 50 (data is exemplarily taken from one cell each).

Already at cycle 5, for the µm-Si-rGO_1.25CMC_3.75SBR electrode significant lower lithiation potentials (and higher delithiation potentials) can be observed due to a higher voltage drop as a result of the lower internal electrical conductivity of the CMC/SBR = 1:3 electrode. This results in a lower specific capacity as the cut-off criteria of 0.01 V is kept constant during constant current cycling.

Furthermore, a difference in the peak-to-peak ratio can be detected between the µm-Si-rGO_2.5CMC_2.5SBR and the µm-Si-rGO_3.75CMC_1.25SBR electrode during the delithiation process (U = 0.01 -> 1.5 V; positive values). The first peak around 0.3 V refers to the $Li_{3.5}Si$ -> $Li_{2.0}Si$ delithiation reaction, while the second refers to the $Li_{2.0}si$ -> Si follow-up reaction. The peak of the follow-up reaction is significant higher for the µm-Si-rGO_2.5CMC_2.5SBR electrode. That means that the loss of active material during the delithiation (shrinkage) is lower here, which confirms the importance of the SBR content for µm-sized Silicon, especially in the course of cycling stability.

In addition, in **Figure S7** the results of the nm-Si-rGO electrodes are shown. The corresponding charge and discharge curves are available in **Figure S10**.

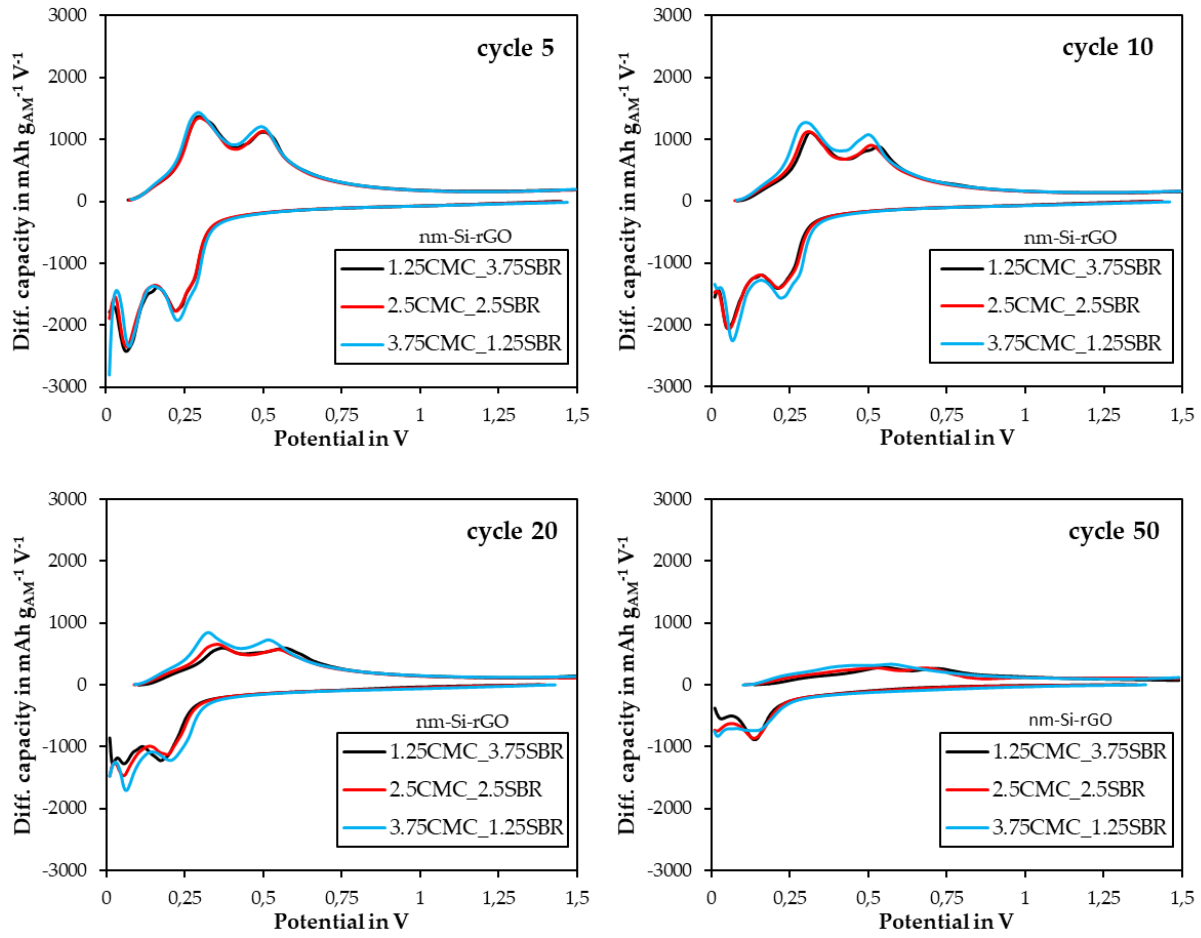

***Figure S7**: Differential capacity over potential for all nm-Si-rGO electrodes for cycle 5, 10, 20 and 50. (data is exemplarily taken from one cell each).*

For the nm-sized Si electrodes the differences are smaller. Nevertheless, it can be observed that the lithiation potential for nm-Si-rGO_3.75CMC_1.25SBR electrode is higher due to the better internal electrical conductivity of the electrode with high CMC content. This again leads to a higher specific capacity, especially at cycle 10 and 20. At cycle 50 the degradation of all electrodes is so high that there is a barely a difference detectable.

Furthermore, we want to point out that we could not detect any size effects during the dispersing process. In the EDX mappings of the prepared electrodes we could detect homogeneous distribution of sodium from the Na-CMC binder for both µm-Si-rGO and nm-Si-rGO electrodes. The results for the 2.5CMC_2.5SBR compositions are given in the Supplementary Information as an example:

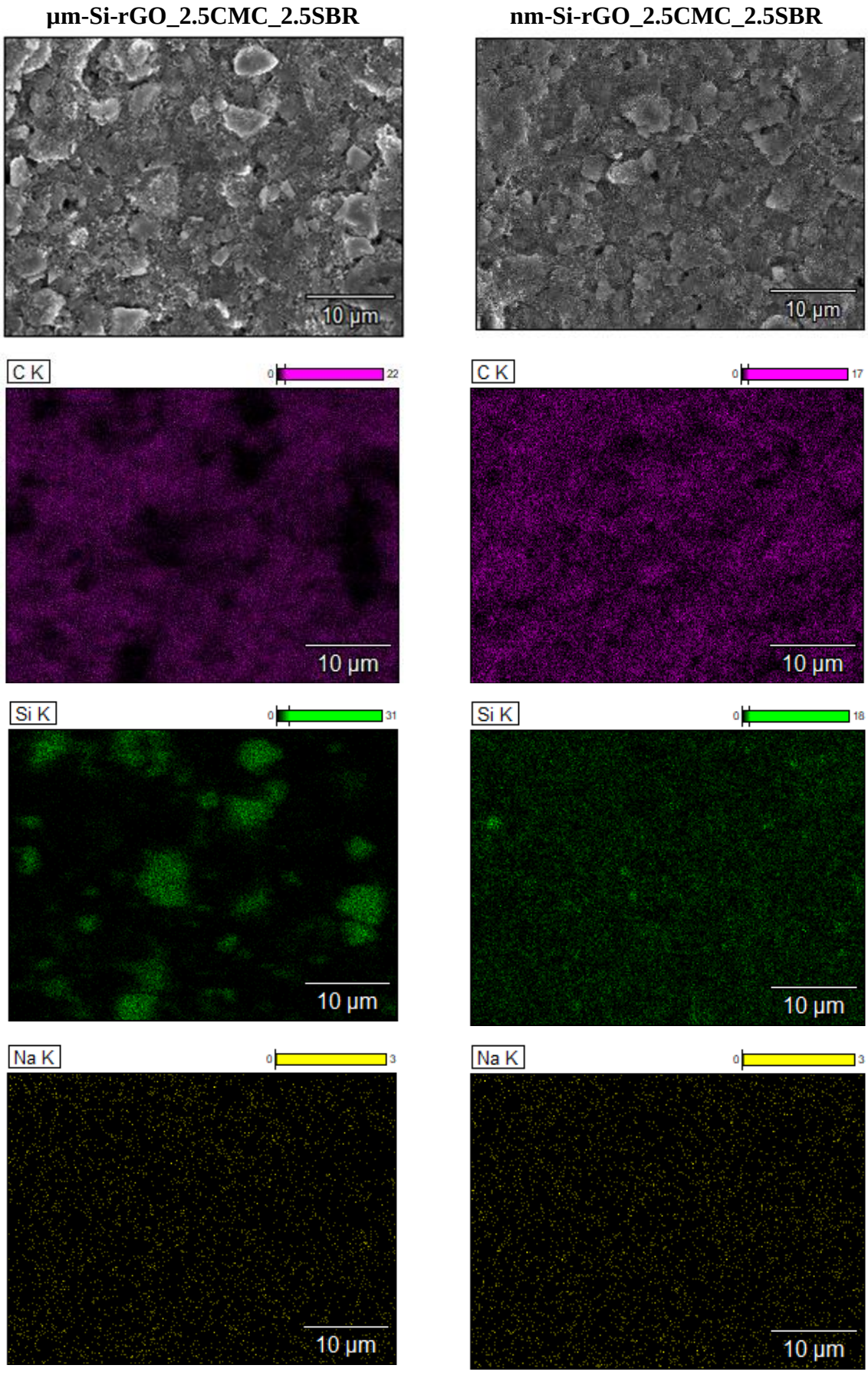

Figure S8: EDX mappings (C, Si and Na) of the µm- and nm-Si-rGO electrodes with the 2.5CMC_2.5SBR binder.

Next, we provide the original charge and discharge curves from which the electrochemical data discussed were calculated for the cycles 1, 5, 10, 20, 50, 55, 60, 65, and 70.

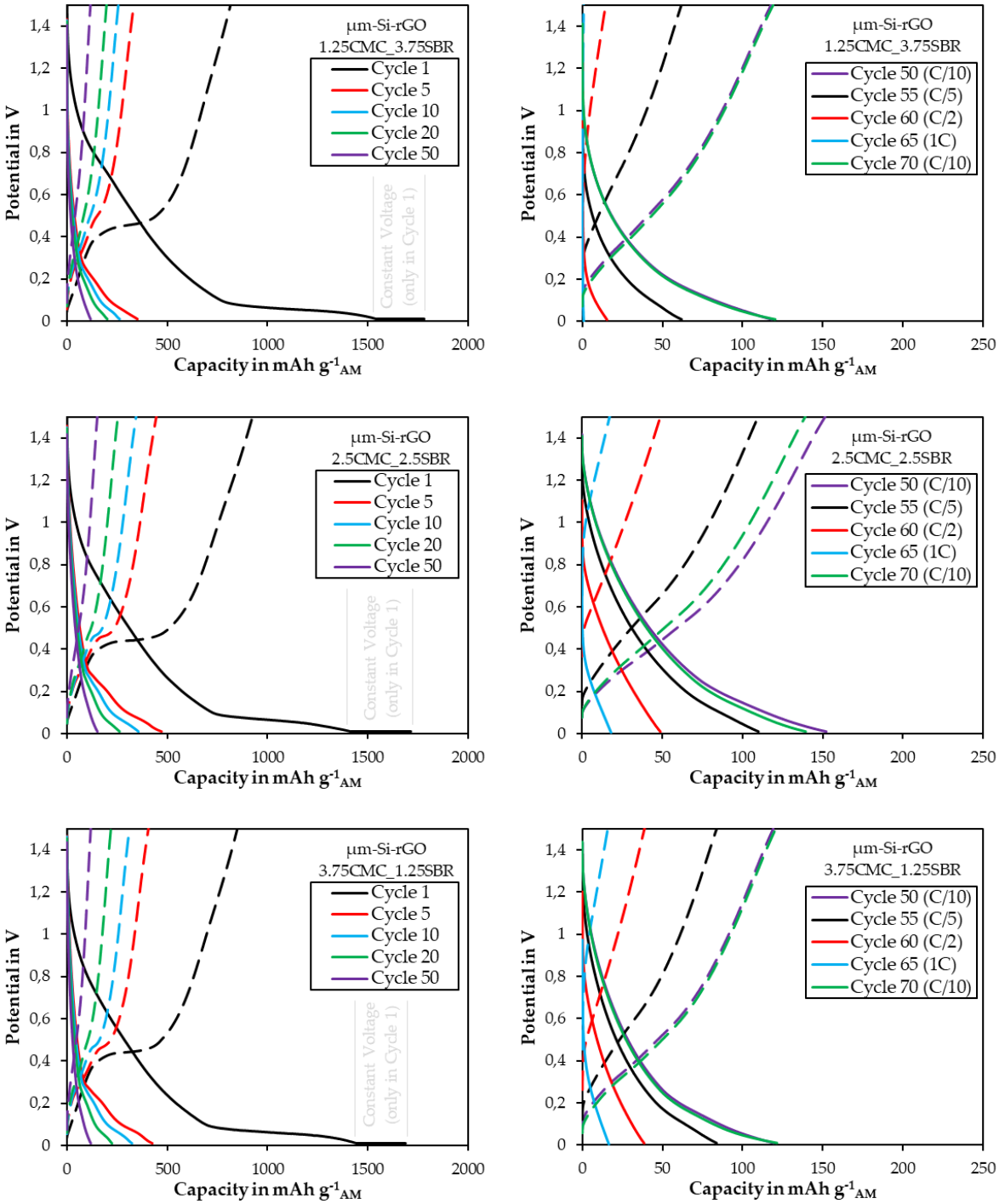

Figure S9: Charge and Discharge curves between the termination criteria 0.01 and 1.5 V for all µm-Si-rGO electrodes in cycle 1, 5, 10, 20 and 50 (at C/10) as well as for the C-rates C/5 (cycle 55), C/2 (cycle 60), 1C (cycle 65) and C/10 again (cycle 70) (data is exemplarily taken from one cell each).

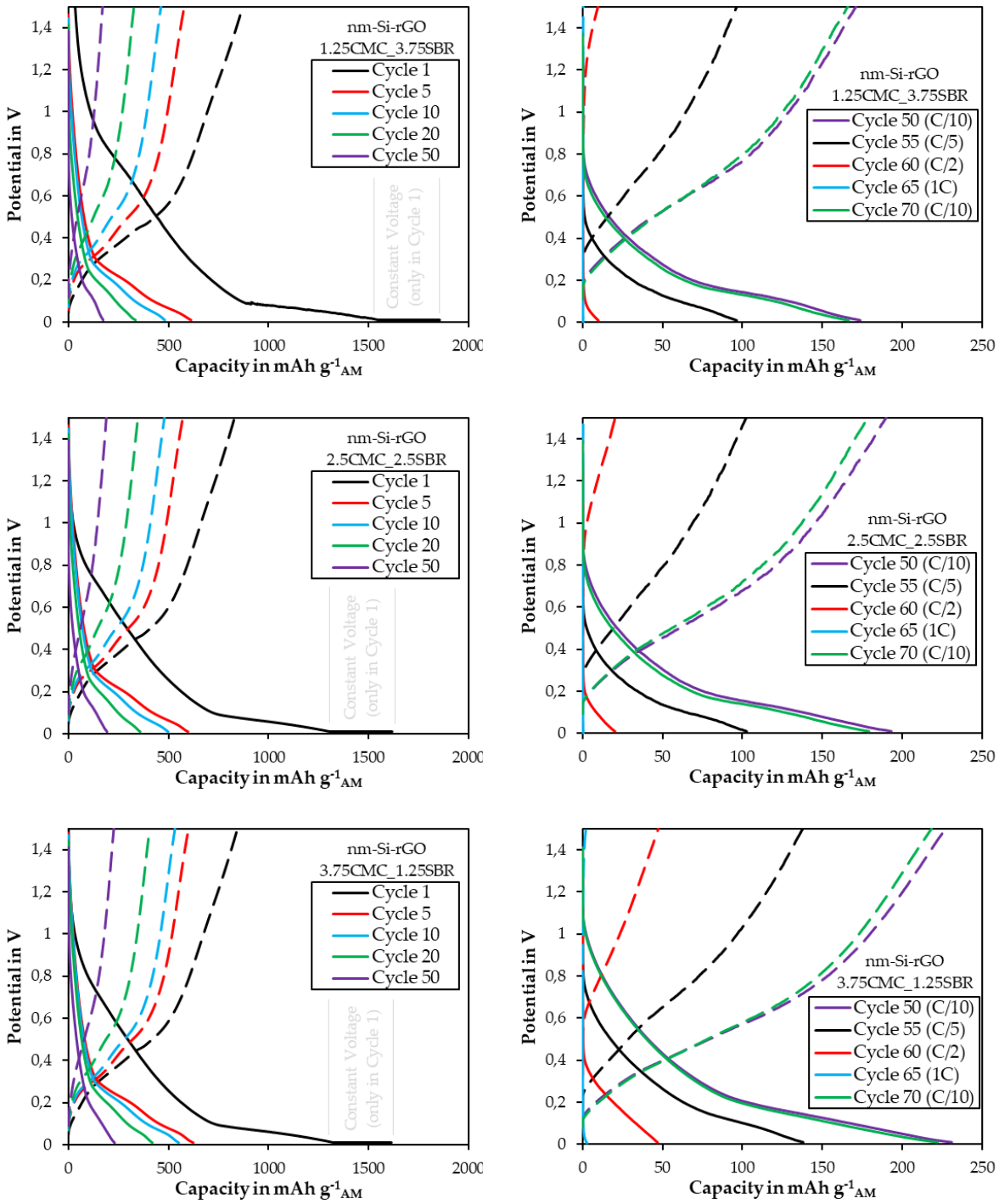

Figure S10: Charge and Discharge curves between the termination criteria 0.01 and 1.5 V for all nm-Si-rGO electrodes in cycle 1, 5, 10, 20 and 50 (at C/10) as well as for the C-rates C/5 (cycle 55), C/2 (cycle 60), 1C (cycle 65) and C/10 again (cycle 70) (data is exemplarily taken from one cell each).

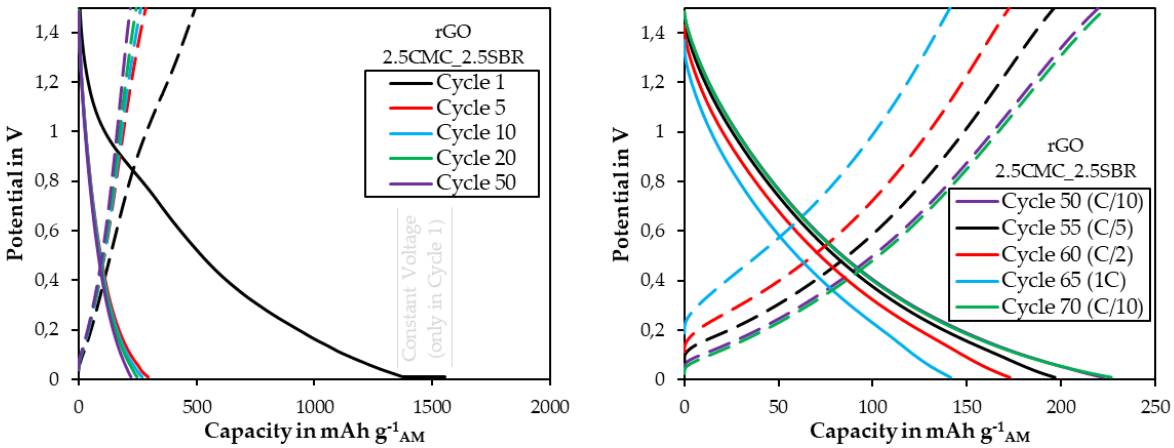

Figure S11: Charge and Discharge curves between the termination criteria 0.01 and 1.5 V for Si-free rGO electrodes in cycle 1, 5, 10, 20 and 50 (at C/10) as well as for the C-rates C/5 (cycle 55), C/2 (cycle 60), 1C (cycle 65) and C/10 again (cycle 70) (data is exemplarily taken from one cell).

Lastly, we give the detailed results of the galvanostatic impedance spectroscopy before and after cycling for the µm-Si-rGO, the nm-Si-rGO as well as the Si-free rGO electrodes.

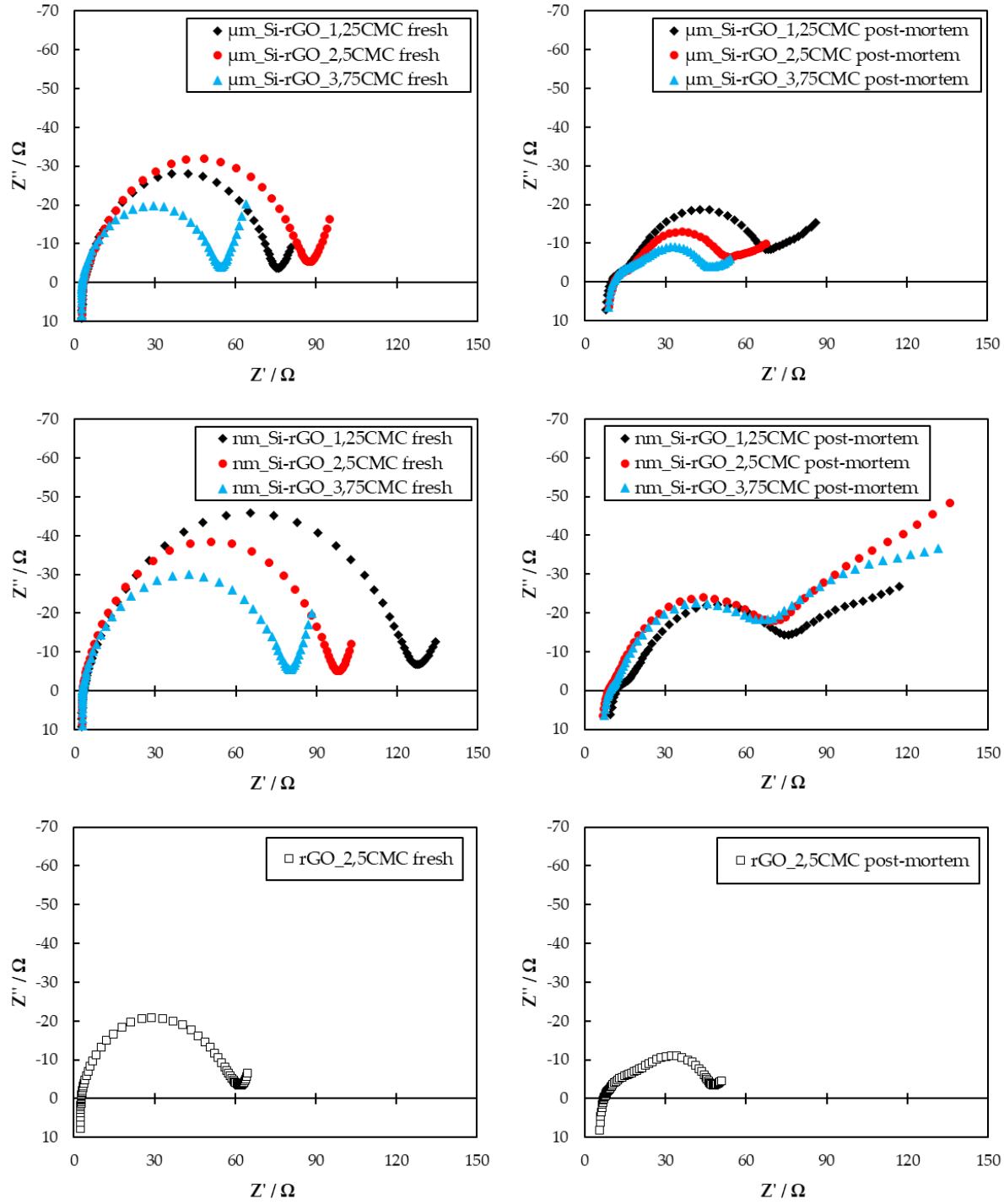

Figure S12: Galvanostatic EIS curves of all investigated electrodes before and after cycling (f = 1 MHz – 0.5 Hz; I = 0.2 mA). The results shown represent the mean values from 3 cells each.